Stability and Dispersion Analysis of Battle–Lemarie-Based MRTD Schemes

Emmanouil M. Tentzeris, *Member, IEEE,* Robert L. Robertson, James F. Harvey, *Member, IEEE,* and Linda P. B. Katehi, *Fellow, IEEE*

***Abstract*— The stability and dispersion performance of the recently developed Battle–Lemarie multiresolution time-domain schemes is investigated for different stencil sizes. The contribution of wavelets is enhanced and analytical expressions for the maximum allowable time step are derived. It is observed that larger stencils decrease the numerical phase error, making it significantly lower than finite-difference time domain for low and medium discretizations. The addition of wavelets further improves the dispersion performance for discretizations close to the Nyquist limit, though it decreases the value of the maximum time step, guaranteeing the stability of the scheme.**

I. Introduction

FINITE-DIFFERENCE time-domain (FDTD) numerical techniques are widely used today for the analysis of various microwave geometries and for the modeling of electromagnetic (EM) wave propagation. Though many of them are very simple to implement and can be easily applied to different topologies with remarkable accuracy, they cause a numerical phase error during the propagation along the discretized grid. For example, the numerical phase velocity in the FDTD [1] can be different from the velocity of light, depending on the cell size as a fraction of the smallest propagating wavelength and the direction of the grid propagation. Thus, a nonphysical dispersion is introduced and affects the accuracy limits of FDTD simulations, especially of large structures.

In addition, it is well known that the finite-difference schemes in time and space domains require that the used time step should take values within an interval that is a function of the cell size. If the time step takes a value outside the bounds of this interval, the algorithm will be numerically unstable, leading to a spurious increase of the field values without limit as the time increases.

Though the stability and the dispersion analysis for the conventional Yee's FDTD algorithm has been thoroughly investigated [2], only a few results have been presented concerning multiresolution time-domain (MRTD) schemes based on cubic spline Battle–Lemarie scaling and wavelet functions [3]. The functions of this family do not have compact support, thus the finite approximations of the derivatives are finite stencil summations instead of finite differences. In this paper, the effect of the stencil size, as well as of the addition of wavelets, is investigated and comparison with second-order and higher order FDTD schemes displays a difference in their respective behaviors.

Manuscript received April 1, 1998. This work was supported by the Army Research Office under Grant C-034796.

E. M. Tentzeris is with the School of Electrical and Computer Engineering, Georgia Institute of Technology, Atlanta, GA 30332-0250 USA.

R. L. Robertson and L. P. B. Katehi are with the Radiation Laboratory, Department of Electrical Engineering and Computer Science, The University of Michigan at Ann Arbor, Ann Arbor, MI 48109-2122 USA.

J. F. Harvey is with the Army Research Office, Research Triangle Park, NC 27009-2211 USA.

Publisher Item Identifier S 0018-9480(99)05288-6.

II. Stability Analysis

For simplicity and without loss of generality, it is assumed throughout the stability and dispersion analysis that the E- and H-fields are expanded only in terms of scaling functions (S-MRTD) in space domain. Hints for the addition of wavelets will be presented where needed. Following the procedure of [3], the MRTD equations for the two-dimensional (2-D) TM^z mode can be written as

$$\frac{{}_{k+1/2}H^x_{i,j-1/2} - {}_{k-1/2}H^x_{i,j-1/2}}{\Delta t} = -\frac{1}{\mu\Delta y}\sum_{j'=-n_a}^{n_a-1} a(j')_k E^z_{i,j+j'}$$

$$\frac{{}_{k+1/2}H^y_{i-1/2,j} - {}_{k-1/2}H^y_{i-1/2,j}}{\Delta t} = \frac{1}{\mu\Delta x}\sum_{i'=-n_a}^{n_a-1} a(i')_k E^z_{i+i',j}$$

$$\frac{{}_{k+1}E^z_{i,j} - {}_{k}E^z_{i,j}}{\Delta t} = \frac{1}{\epsilon}\left[\frac{1}{\Delta x}\sum_{i'=-n_a}^{n_a-1} a(i')_{k+1/2}H^y_{i+i'-1/2,j} - \frac{1}{\Delta y}\sum_{j'=-n_a}^{n_a-1} a(j')_{k+1/2}H^x_{i,j+j'-1/2}\right].$$

Following the stability analysis described in [4], these equations are decomposed into separate time and space eigenvalue problems. The finite-difference approximations of the time derivatives on the left-hand side of the equations can be written

as an eigenvalue problem

$$\frac{{}^{k+1/2}H^x_{i,j-1/2} - {}^{k-1/2}H^x_{i,j-1/2}}{\Delta t} = \Lambda_k H^x_{i,j-1/2} \quad (1)$$

$$\frac{{}^{k+1/2}H^y_{i-1/2,j} - {}^{k-1/2}H^y_{i-1/2,j}}{\Delta t} = \Lambda_k H^y_{i-1/2,j} \quad (2)$$

$$\frac{{}^{k+1}E^z_{i,j} - {}^{k}E^z_{i,j}}{\Delta t} = \Lambda_{k+1/2} E^z_{i,j}. \quad (3)$$

In order to avoid instability during normal time stepping, the imaginary part of Λ, $\mathrm{Imag}(\Lambda)$, must satisfy

$$-\frac{2}{\Delta t} \le \mathrm{Imag}(\Lambda) \le \frac{2}{\Delta t}. \quad (4)$$

For each time step k, the instantaneous value of the electric and magnetic fields distributed in space across the grid can be Fourier transformed with respect to the i- and j-coordinates to provide a spectrum of sinusoidal modes (plane-wave eigenmodes of the grid). Assuming an eigenmode of the spectral domain with k_x and k_y being the x- and y-components of the numerical eigenvector, the field components can be written as

$$E^z_{I,J} = E_{z_o} e^{j(k_x I\Delta x + k_y J\Delta y)}$$
$$H^x_{I,J-1/2} = H_{x_o} e^{j(k_x I\Delta x + k_y (J-1/2)\Delta y)}$$
$$H^y_{I-1/2,J} = H_{y_o} e^{j(k_x (I-1/2)\Delta x + k_y J\Delta y)}.$$

Substituting these expressions to (1)–(3) and applying Euler's identity, we get

$$\Lambda^2 = -\frac{4}{\mu\epsilon}\left[\frac{1}{(\Delta x)^2}\left(\sum_{i'=0}^{n_a-1} a(i')\,\sin\Big(k_x(i'+1/2)\Delta x\Big)^2\right) + \frac{1}{(\Delta y)^2}\left(\sum_{j'=0}^{n_a-1} a(j')\,\sin\Big(k_y(j'+1/2)\Delta y\Big)\right)^2\right]. \quad (5)$$

In (5), Λ is a pure imaginary, which is bounded for any wave vector $k = (k_x, k_y)$

$$-2c\left(\sum_{i'=0}^{n_a-1}|a(i')|\right)\sqrt{\frac{1}{(\Delta x)^2}+\frac{1}{(\Delta y)^2}} \le \mathrm{Imag}(\Lambda) \le 2c\left(\sum_{i'=0}^{n_a-1}|a(i')|\right)\sqrt{\frac{1}{(\Delta x)^2}+\frac{1}{(\Delta y)^2}} \quad (6)$$

where $c = (1/\sqrt{\mu\epsilon})$ is the velocity of the light in the modeled medium.

Numerical stability is maintained for every spatial mode only when the range of eigenvalues given by (6) is contained entirely within the stable range of time-differentiation eigenvalues given by (4). Since both ranges are symmetrical around zero, it is adequate to set the upper bound of (6) to be smaller or equal to (4), giving

$$\Delta t \le \frac{1}{c\left(\sum_{i'=0}^{n_a-1}|a(i')|\right)\sqrt{\frac{1}{(\Delta x)^2}+\frac{1}{(\Delta y)^2}}}. \quad (7)$$

For $\Delta x = \Delta y = \Delta$, the above stability criterion gives

$$\Delta t_{\text{S-MRTD}} \le s_{SS}\frac{\Delta}{c\sqrt{2}} \quad (8)$$

where

$$s_{SS} = \frac{1}{\sum_{i'=0}^{n_a-1}|a(i')|}. \quad (9)$$

It is known [2] that

$$\Delta t_{\text{FDTD}} \le \frac{1}{c\sqrt{\frac{1}{(\Delta x)^2}+\frac{1}{(\Delta y)^2}}} \quad (10)$$

which for $\Delta x = \Delta y = \Delta$ gives

$$\Delta t_{\text{FDTD}} \le \frac{\Delta}{c\sqrt{2}}. \quad (11)$$

Equations (8)–(11) show that for the same discretization size, the upper bounds of the time steps of FDTD and S-MRTD are comparable and related through the factor s_{SS}. The stability analysis can be generalized easily to three dimensions. The new stability criteria can be derived by (8) and (11) by substituting the term $\sqrt{2}$ with $\sqrt{3}$.

More complicated expressions can be derived for the maximum allowable time step for schemes containing scaling and wavelet functions. For simplicity and without loss of generality, it is assumed that the stencil size is equal for all three summations ($n_a = n_b = n_c = n$). The upper bound of the time step for the 2-D MRTD scheme with zero-resolution wavelets to one (x-direction) or two directions (x- and y-directions) for $\Delta x = \Delta y = \Delta$ is given by

$$\Delta t_{W_0\text{S-MRTD,max}} \approx s_{W_0 S}\frac{\Delta}{c\sqrt{2}} \quad (12)$$

with (13), shown at the bottom of this page, and

$$\Delta t_{W_0W_0\text{-MRTD,max}} \approx s_{W_0W_0}\frac{\Delta}{c\sqrt{2}} \quad (14)$$

$$s_{W_0S} = \frac{2}{\sqrt{3\left(\sum_{i'}|a|\right)^2 + \left(\sum_{i'}|b_0|\right)^2 + 2\left(\sum_{i'}|c_0|\right)^2 + \left(\sum_{i'}|a+b_0|\right)\sqrt{\left(\sum_{i'}|a-b_0|\right)^2 + 4\left(\sum_{i'}|c_0|\right)^2}}} \quad (13)$$

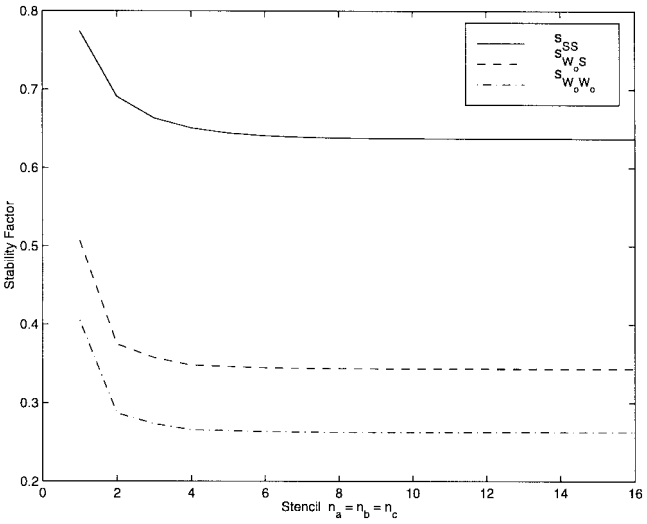

Fig. 1. Stability parameter s for MRTD.

with (15), shown at the bottom of this page, where the notation

$$\sum_{k'} |x| = \sum_{k'=0}^{n-1} |x(k')| \tag{16}$$

has been used. Values for the coefficients b_0, c_0 are given in [3].

It can be observed that the upper bound of the time step depends on the stencil size n_a, n_b, n_c. This dependence is expressed through the coefficients s_{SS}, s_{W_0S}, $s_{W_0W_0}$, which decrease as the stencil size increases. Fig. 1 shows that s_{SS} practically converges to the value 0.6371 after $n_a \geq 10$ and $s_{W_0S} \approx 0.3433$ and $s_{W_0W_0} \approx 0.2625$ for $n_a = n_b = n_c \geq 10$. The expression of s_{SS} can be easily derived by the expressions of s_{W_0S} and $s_{W_0W_0}$ by zeroing out the effect of b_0, c_0.

III. Dispersion Analysis

To calculate the numerical dispersion of the S-MRTD scheme, plane monochromatic traveling-wave trial solutions are substituted in the discretized Maxwell's equations. For example, the E_z component for the TM^z mode has the form

$$_kE^z_{I,J} = E_{z_o} e^{j(k_x I\Delta x + k_y J\Delta y - \omega k\Delta t)} \tag{17}$$

where k_x and k_y are the x- and y-components of the numerical wave vector and ω is the wave angular frequency. Substituting the above expressions into (1)–(3), the following numerical dispersion relation is obtained for the TM^z mode of the S-MRTD scheme after algebraic manipulation:

$$\left[\frac{1}{c\Delta t}\sin\left(\frac{\omega\Delta t}{2}\right)\right]^2 = \left[\frac{1}{\Delta x}\left(\sum_{i'=0}^{n_a-1} a(i')\sin\Big(k_x(i'+1/2)\Delta x\Big)\right)\right]^2 + \left[\frac{1}{\Delta y}\left(\sum_{j'=0}^{n_a-1} a(j')\sin\Big(k_y(j'+1/2)\Delta y\Big)\right)\right]^2. \tag{18}$$

For square unit cells ($\Delta x = \Delta y = \Delta$) and wave propagating at an angle ϕ with respect to x-axis ($k_x = k\cos\phi$ and $k_y = k\sin\phi$), the above expression is simplified to

$$\left[\frac{\Delta}{c\Delta t}\sin\left(\frac{\omega\Delta t}{2}\right)\right]^2 = \left(\sum_{i'=0}^{n_a-1} a(i')\sin\Big(k\cos\phi(i'+1/2)\,\Delta\Big)\right)^2 + \left(\sum_{j'=0}^{n_a-1} a(j')\sin\Big(k\sin\phi(j'+1/2)\,\Delta\Big)\right)^2. \tag{19}$$

TABLE I
Coefficients C_i for Different MRTD Schemes

Scheme	C_1	C_2	C_3	C_4	C_5	C_6
SS	$\neq 0$	0	0	$\neq 0$	0	0
W_0S	$\neq 0$	0	0	$\neq 0$	$\neq 0$	$\neq 0$
SW_0	$\neq 0$	$\neq 0$	$\neq 0$	$\neq 0$	0	0
W_0W_0	$\neq 0$	$\neq 0$	$\neq 0$	$\neq 0$	$\neq 0$	$\neq 0$

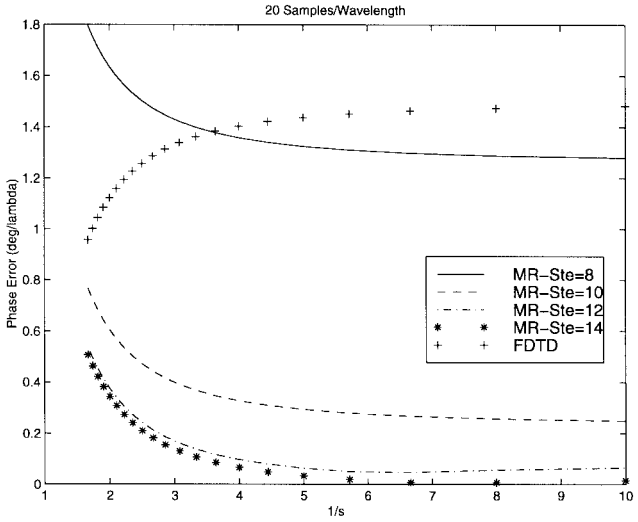

Fig. 2. Dispersion characteristics of S-MRTD for various stencils (20 samples/λ).

$$s_{W_0W_0} = \frac{2}{\sqrt{2\left(\sum_{i'}|a|\right)^2 + 2\left(\sum_{i'}|b_0|\right)^2 + 4\left(\sum_{i'}|c_0|\right)^2 + 2\left(\sum_{i'}|a+b_0|\right)\sqrt{\left(\sum_{i'}|a-b_0|\right)^2 + 4\left(\sum_{i'}|c_0|\right)^2}}} \tag{15}$$

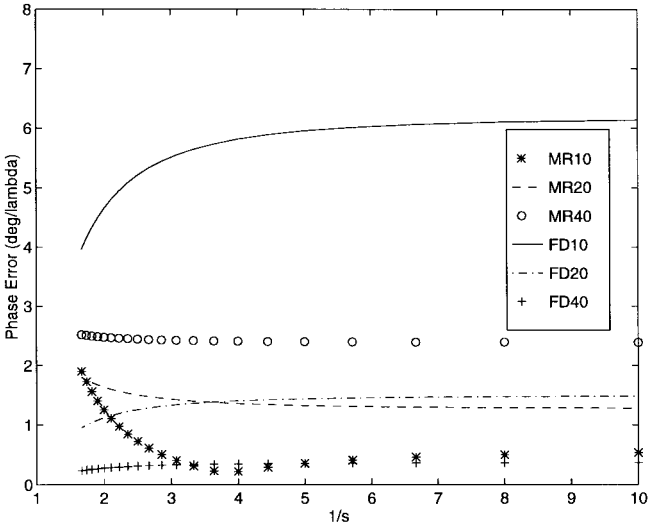

Fig. 3. Dispersion characteristics of S-MRTD for $n_a = 8$. Phase error ($\mathrm{Ste} = 8$ versus FDTD).

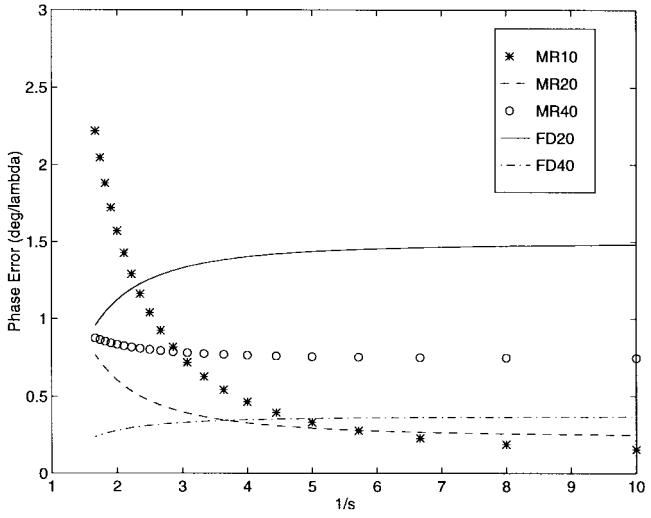

Fig. 4. Dispersion characteristics of S-MRTD for $n_a = 10$. Phase error ($\mathrm{Ste} = 10$ versus FDTD).

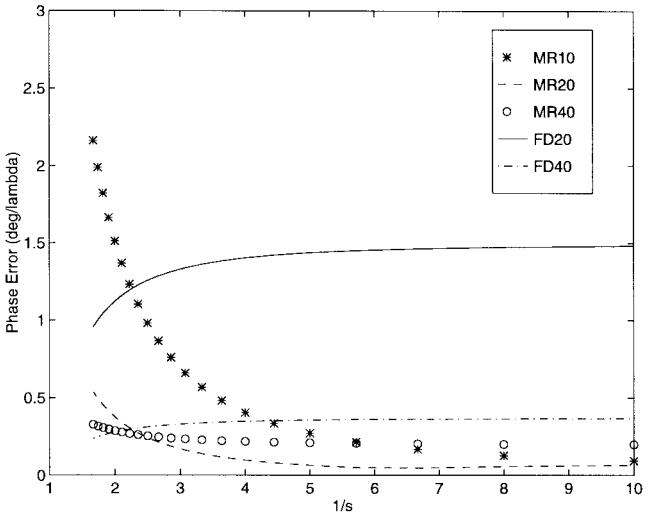

Fig. 5. Dispersion characteristics of S-MRTD for $n_a = 12$. Phase error ($\mathrm{Ste} = 12$ versus FDTD).

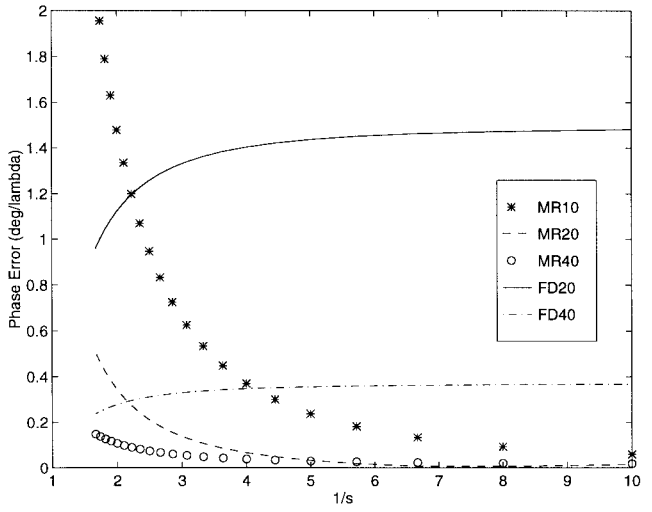

Fig. 6. Dispersion characteristics of S-MRTD for $n_a = 14$. Phase error ($\mathrm{Ste} = 14$ versus FDTD).

This equation relates the numerical wave vector, wave frequency, cell size, and time step. Numerical solutions of (19) for different angles, time-step sizes, and frequencies quantify the dispersion characteristics.

Defining the Courant number $q = (c\Delta t)/\Delta$ and the number of cells per wavelength $n_l = \lambda_{\mathrm{REAL}}/\Delta$ and using the definition of the wave vector $k = (2\pi)/\lambda_{\mathrm{NUM}}$, the dispersion relationship can be written as

$$\left[\frac{1}{q}\,\sin(\pi q/n_l)\right]^2 = \left[\sum_{i'=0}^{n_a-1} a(i')\,\sin\Big(\pi u(2i'+1)\,\cos\phi/n_l\Big)\right]^2 + \left[\sum_{j'=0}^{n_a-1} a(j')\,\sin\Big(\pi u(2j'+1)\,\sin\phi/n_l\Big)\right]^2 \tag{20}$$

where $u = \lambda_{\mathrm{REAL}}/\lambda_{\mathrm{NUM}}$ is the ratio of the theoretically given value to the numerical value of the propagating wavelength and expresses the phase error introduced by the S-MRTD algorithm. To satisfy the stability requirements, q has to be smaller than 0.45 $(= 0.6371/\sqrt{2})$ for the 2-D simulations.

The above analysis can be extended to cover the expansion in scaling and zero-resolution wavelet functions in x- and y- or both directions.

The general dispersion relationship is

$$\frac{\mu}{\epsilon}\,(C_1C_1 + C_2C_2 + C_4C_4 + C_5C_5) + \left(\frac{\mu}{\epsilon}\right)^2\left[\frac{(C_4C_5 + C_5C_6)^2}{A} + \frac{(C_1C_2 + C_2C_3)^2}{B}\right] + \left(\frac{\mu}{\epsilon}\right)^4 (C_1C_2 + C_2C_3)^2(C_4C_5 + C_5C_6)^2 \cdot \left(\frac{1}{A} + \frac{1}{B}\right)^2 \frac{1}{F} = 1 \tag{21}$$

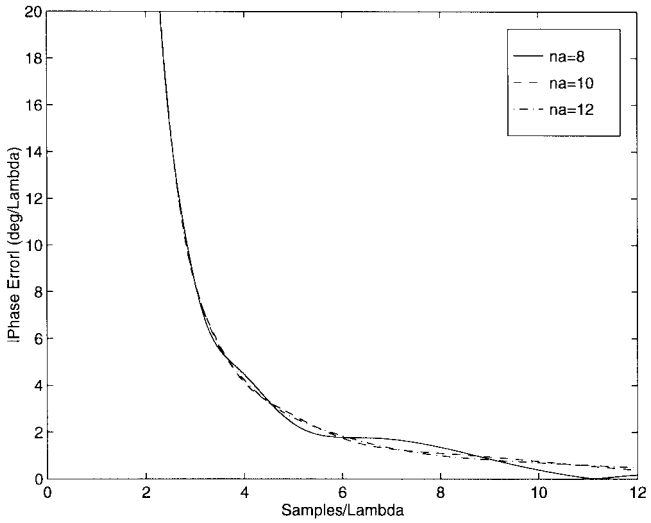

Fig. 7. Stencil effect on the dispersion characteristics of S-MRTD (sparse grid).

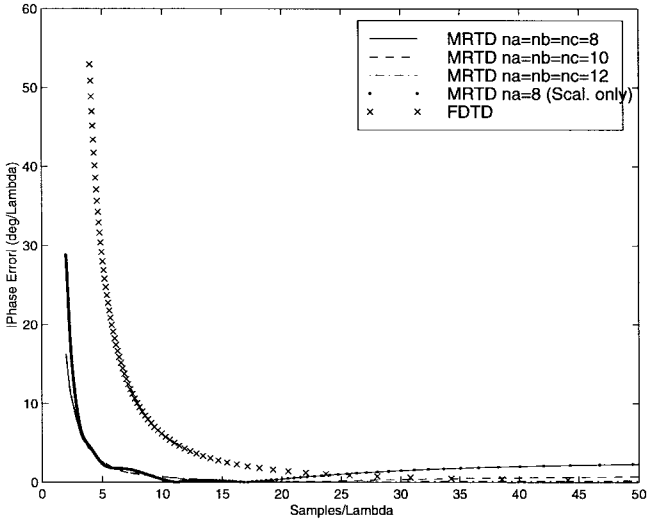

Fig. 9. Wavelets effect on the dispersion characteristics of MRTD for various stencils.

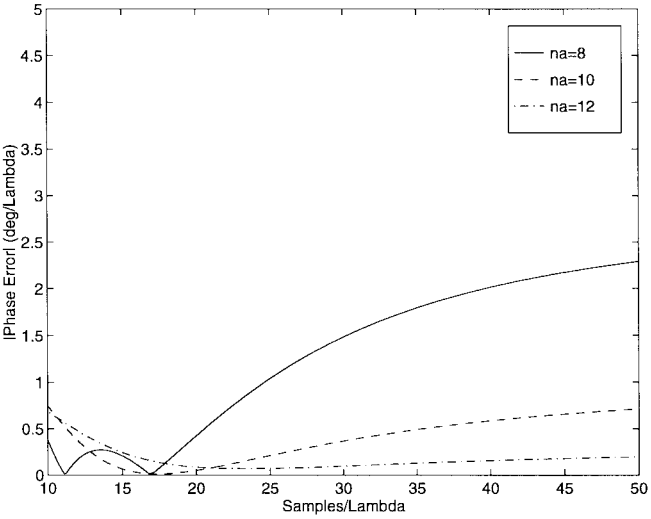

Fig. 8. Stencil effect on the dispersion characteristics of S-MRTD (dense grid).

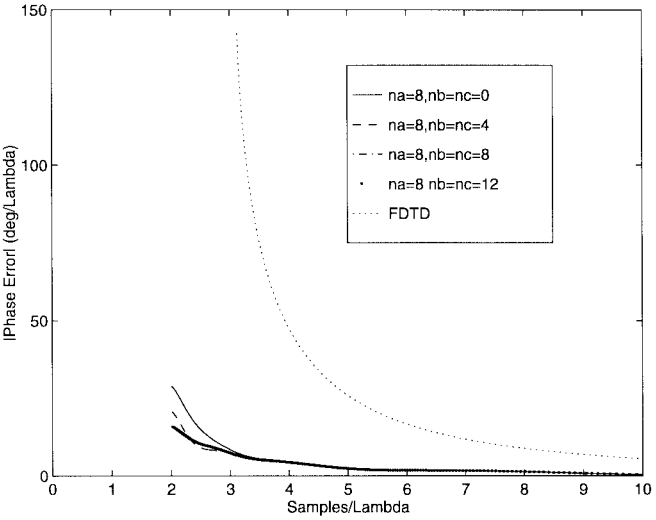

Fig. 10. Wavelets effect on the dispersion characteristics of MRTD for $n_a = 8$ (coarse grid).

with

$$F = 1 - \left[\frac{\mu}{\epsilon}\,(C_1C_2 + C_2C_3)\right]^2 \frac{1}{A} - \left[\frac{\mu}{\epsilon}(C_4C_5 + C_5C_6)\right]^2 \frac{1}{B} - \left[\frac{\mu}{\epsilon}(C_2C_2 + C_3C_3 + C_5C_5 + C_6C_6\right]$$

$$A = 1 - \frac{\mu}{\epsilon}(C_1C_1 + C_2C_2 + C_5C_5 + C_6C_6)$$

$$B = 1 - \frac{\mu}{\epsilon}(C_2C_2 + C_3C_3 + C_4C_4 + C_5C_5). \tag{22}$$

C_i is defined by

$$C_1 = -\frac{\Delta t}{\mu\Delta\,\sin(\omega\Delta t/2)} \sum_{j'=0}^{n_a} a(j')\,\sin\Big(k_y(j'+1/2)\Delta\Big)$$

$$C_2 = -\frac{\Delta t}{\mu\Delta\,\sin(\omega\Delta t/2)} \sum_{j'=0}^{n_c} c_0(j')\,\sin(k_y j'\Delta)$$

$$C_3 = -\frac{\Delta t}{\mu\Delta\,\sin(\omega\Delta t/2)} \sum_{j'=0}^{n_b} b_0(j')\,\sin\Big(k_y(j'+1/2)\Delta\Big)$$

$$C_4 = -\frac{\Delta t}{\mu\Delta\,\sin(\omega\Delta t/2)} \sum_{i'=0}^{n_a} a(i')\,\sin\Big(k_x(i'+1/2)\Delta\Big)$$

$$C_2 = -\frac{\Delta t}{\mu\Delta\,\sin(\omega\Delta t/2)} \sum_{i'=0}^{n_c} c_0(i')\,\sin(k_x i'\Delta)$$

$$C_3 = -\frac{\Delta t}{\mu\Delta\,\sin(\omega\Delta t/2)} \sum_{i'=0}^{n_b} b_0(i')\,\sin\Big(k_x(i'+1/2)\Delta\Big). \tag{23}$$

Equation (21) can be applied to the dispersion analysis of SS (only scaling functions), W_0S (zero-resolution wavelets only to x-direction), SW_0 (zero-resolution wavelets only to y-direction) and W_0W_0 (zero-resolution wavelets to both x- and y-directions) following Table I. In case $C_i \neq 0$, it can be calculated by (23).

The above equation is solved numerically by use of Bisection–Newton–Raphson hybrid technique for different values of $n_a, n_b,\ n_c\ n_l, \phi,$ and q. Fig. 2 demonstrates the effect

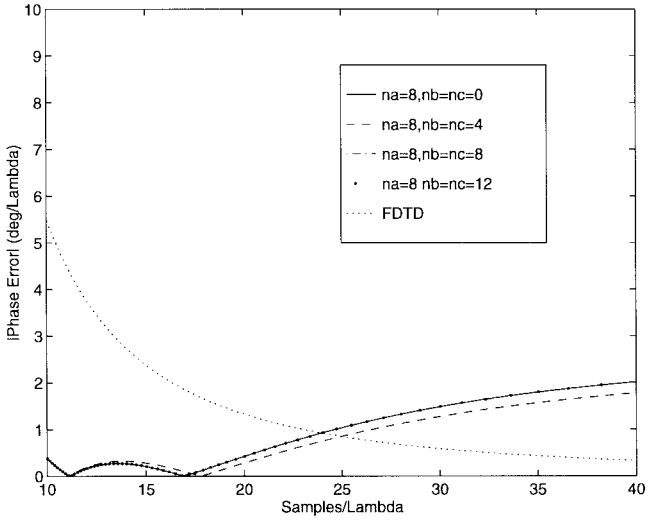

Fig. 11. Wavelets effect on the dispersion characteristics of MRTD for $n_a = 8$ (denser grid).

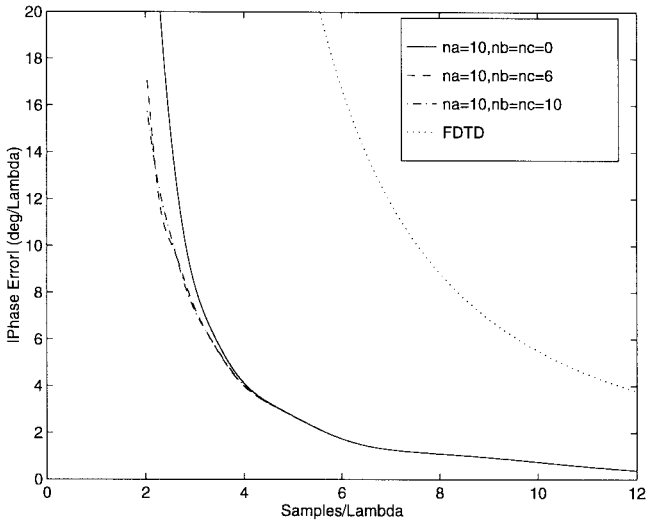

Fig. 12. Wavelets effect on the dispersion characteristics of MRTD for $n_a = 10$ (coarse grid).

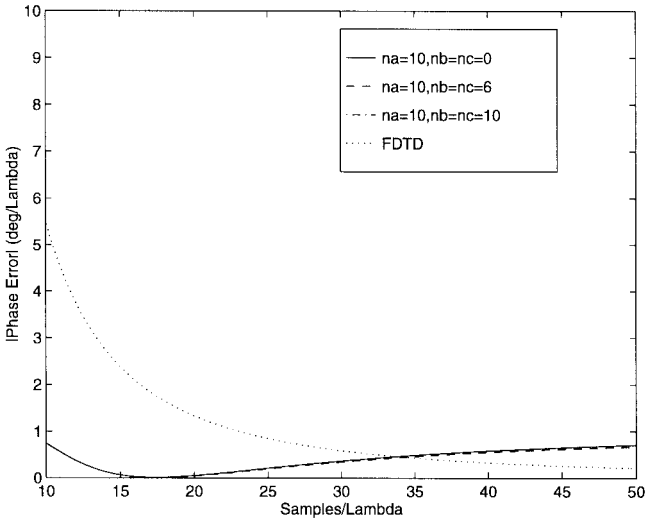

Fig. 13. Wavelets effect on the dispersion characteristics of MRTD for $n_a = 10$ (denser grid).

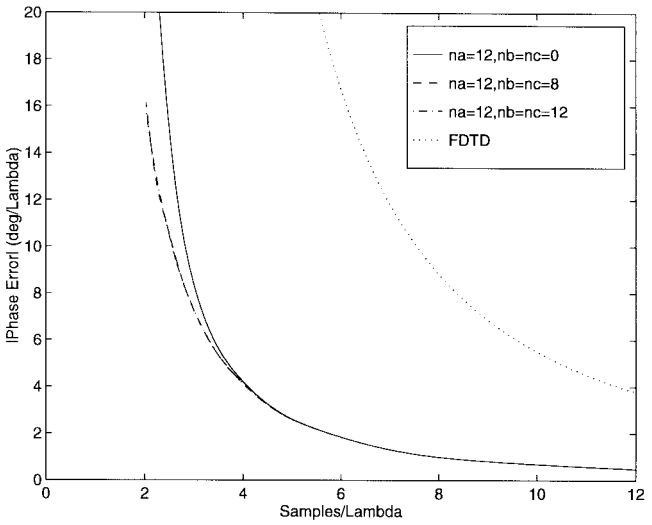

Fig. 14. Wavelets effect on the dispersion characteristics of MRTD for $n_a = 12$ (coarse grid).

of different stencils on the numerical phase error for the S-MRTD scheme and for a discretization of $20\ \mathrm{samples}/\lambda$. Figs. 3–6 show the variation of the numerical phase velocity as a function of the inverse of the Courant number $1/s = 1/q$ for stencil sizes $n_a = n_b = n_c = 8$, 10, 12, 14. For each figure, the following three different discretization sizes are used:

1) 10 cells/wavelength (coarse);
2) 20 cells/wavelength (normal);
3) 40 cells/wavelength (dense).

The results are compared to the respective values of conventional FDTD. It can be observed that the phase error for FDTD decreases quadratically. The variation of the phase error in MRTD exhibits some unique features. For any stencil size, the numerical phase error for MRTD discretization of $10\ \mathrm{cells}/\lambda$ is smaller than that of the FDTD discretization of $10\ \mathrm{cells}/\lambda$ for all values of s and smaller than that of the FDTD discretization of $20\ \mathrm{cells}/\lambda$ for $1/s > 2.5$. Nevertheless, the MRTD error does not decrease monotonically [5] as the cell size is getting smaller. It decreases up to a certain discretization value and then it starts increasing. This value depends on the stencil size and takes larger values for larger stencils. For example, this value is between 10–20 cells/λ for stencil equal to ten, between 20–40 cells/λ for stencil equal to 12, and very close to $40\ \mathrm{cells}/\lambda$ for stencil equal to 14, and can be used as a criterion to characterize the discretization range that the MRTD offers significantly better numerical phase performance than the FDTD.

The phase error caused by the dispersion is cumulative and represents a limitation of the conventional FDTD Yee algorithm for the simulation of electrically large structures. It can be observed that the error of S-MRTD is significantly lower, allowing the modeling of larger structures. FDTD is derived be expanding the fields in pulse basis. As is well known, the Fourier transform of the pulse is a highly oscillating Si(x). On the contrary, the Fourier transform of the Battle–Lemarie cubic spline is similar to a low-pass filter. That

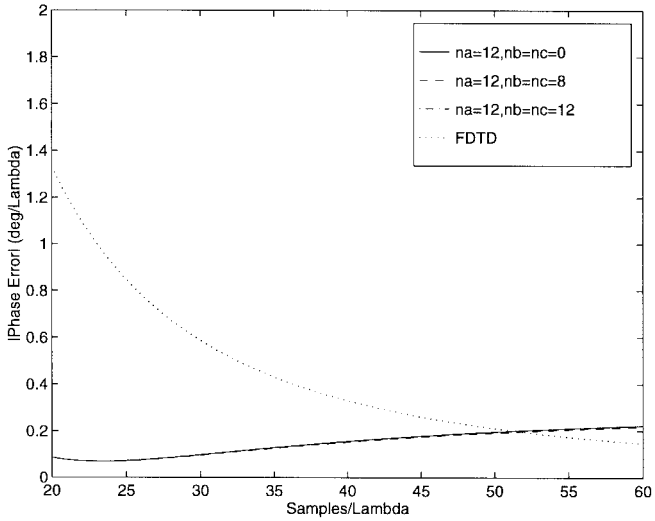

Fig. 15. Wavelets effect on the dispersion characteristics of MRTD for $n_a = 12$ (denser grid).

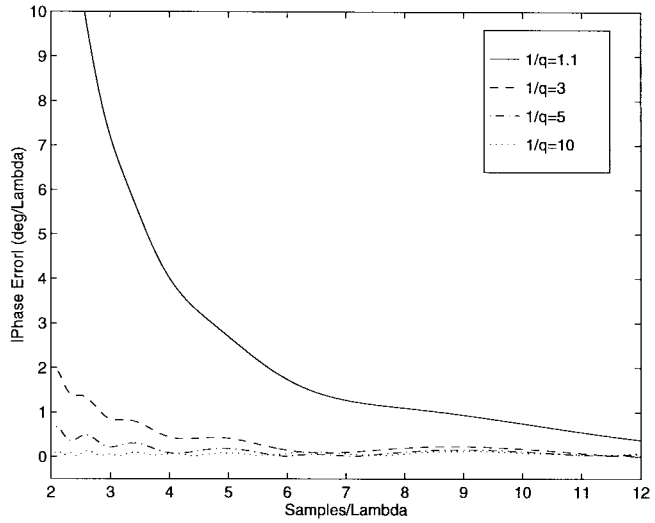

Fig. 16. Effect of the Courant number on the dispersion characteristics of $W_0 - \mathrm{MRTD}$ for $n_a = n_b = n_c = 10$ (coarse grid).

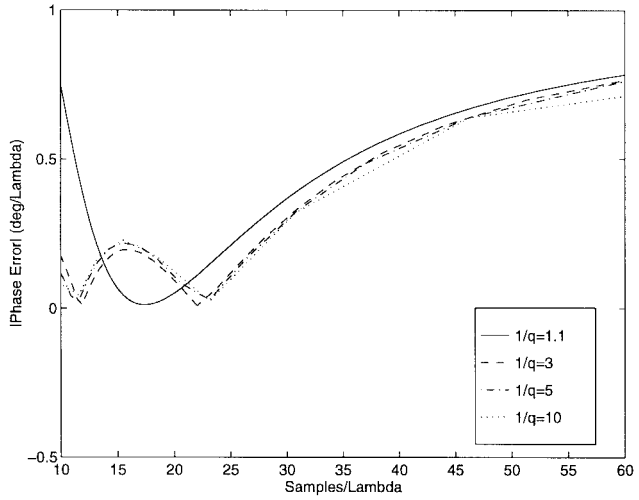

Fig. 17. Effect of the Courant number on the dispersion characteristics of $W_0 - \mathrm{MRTD}$ for $n_a = n_b = n_c = 10$ (denser grid).

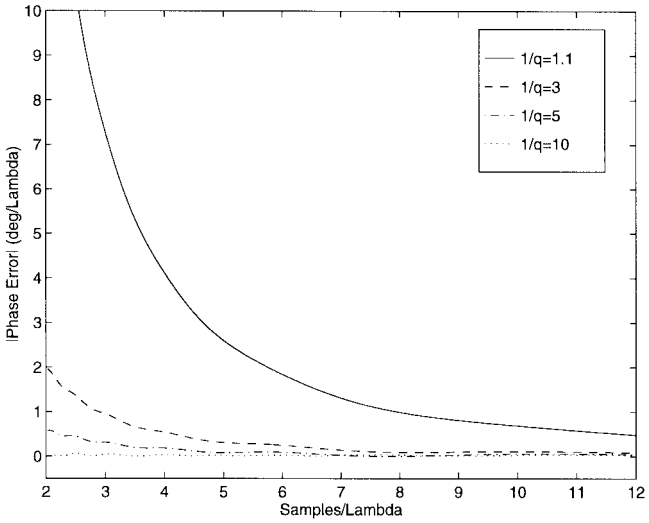

Fig. 18. Effect of the Courant number on the dispersion characteristics of $W_0 - \mathrm{MRTD}$ for $n_a = n_b = n_c = 12$ (coarse grid).

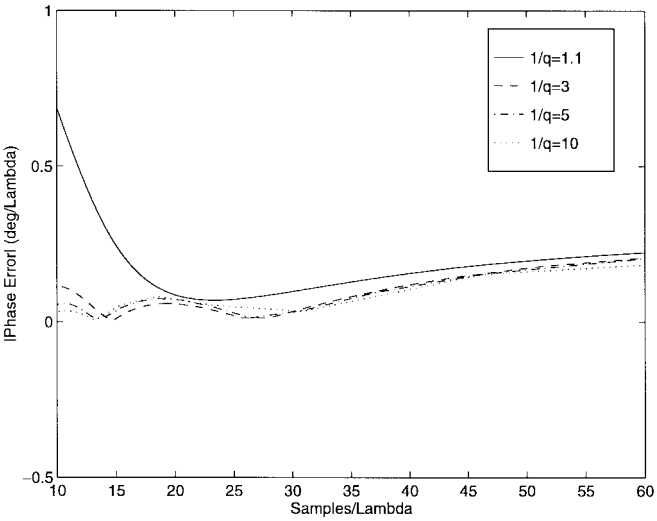

Fig. 19. Effect of the Courant number on the dispersion characteristics of $W_0 - \mathrm{MRTD}$ for $n_a = n_b = n_c = 12$ (denser grid).

"smooth" spectral characteristic offers a much lower phase error even for very coarse (close to 3–4 cells/λ) cells.

By using a larger stencil n_a, the entire-domain oscillating nature of the scaling functions is better represented. Thus, smoother performance for low discretizations (Fig. 7) and lower phase error for higher discretizations (Fig. 8) is achieved as n_a increases from 8 to 12. Wavelets contribute to the improvement of the dispersion characteristics for even coarser cells (close to 2.2–2.4 cells/λ) as is shown in Figs. 9–15. For discretizations above 4 cells/λ the effect of the wavelets is negligible. Figs. 13 and 15 clearly show that the phase error has a minimum for a specific discretization (17 for $n_a = 10$ and 25 for $n_a = 12$).

Figs. 16–19 show that, for discretizations smaller than 30 cells/λ, the choice of the Courant number significantly affects the dispersion performance that starts converging to the minimum numerical phase error ($0.8°/\lambda$ for $n_a = n_b =$

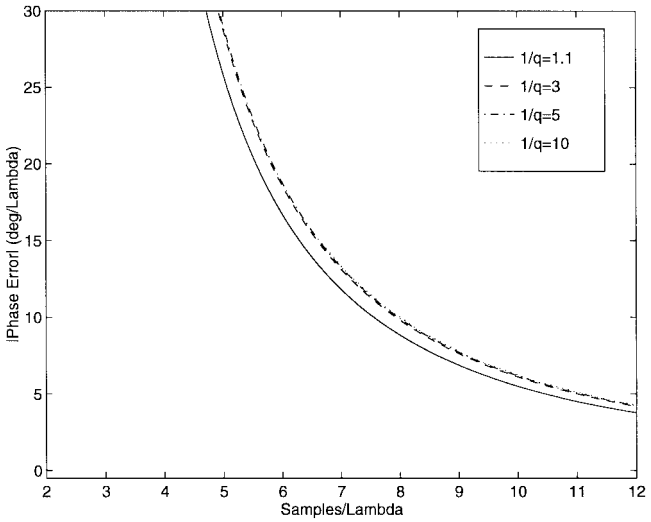

Fig. 20. Effect of the Courant number on the dispersion characteristics of FDTD (coarse grid).

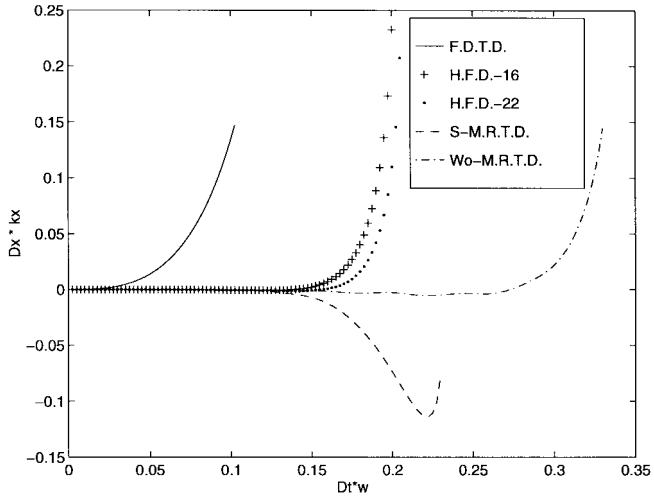

Fig. 22. Comparison of the dispersion performance of S-MRTD and Wo-MRTD with different higher order Yee's schemes.

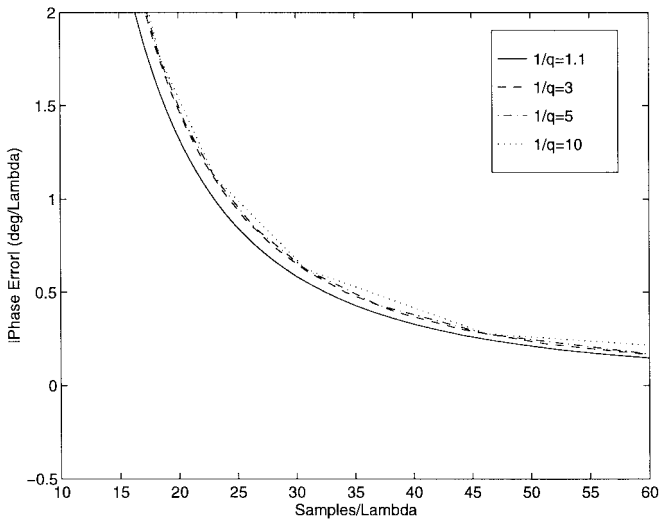

Fig. 21. Effect of the Courant number on the dispersion characteristics of FDTD (denser grid).

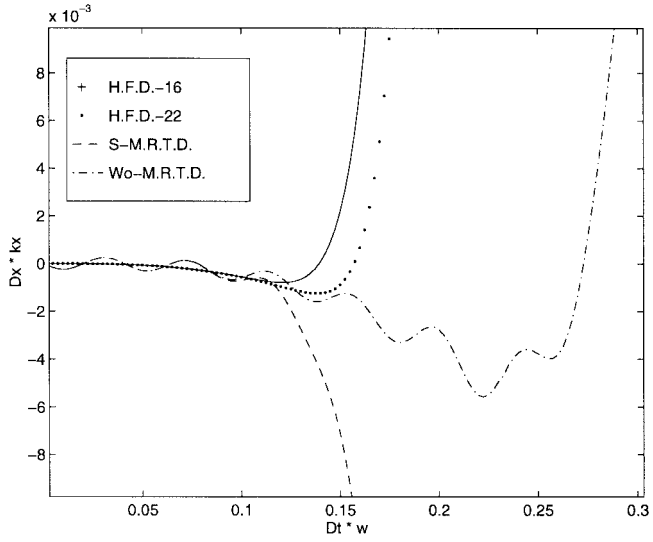

Fig. 23. Details of Fig. 20.

$n_c = 10$ and $0.2°/\lambda$ for $n_a = n_b = n_c = 12$) for $1/q$ close to ten. On the contrary, the FDTD dispersion is almost independent of the Courant number (see Figs. 20 and 21).

It has been claimed in [6] that the S-MRTD Scheme is slightly oscillating and its performance is only comparable with the 14th-order-accuracy Yee's scheme. Though this is true for the S-MRTD schemes with stencil size of eight, the comparison of the dispersion diagrams of Yee's FDTD scheme, Yee's 16th-order (HFD-16) and 22th-order (HFD-22) and S-MRTD and MRTD using zero-resolution wavelets in space-domain (Wo-MRTD) schemes with different stencils leads to interesting results. For validation purposes, the values of $\Delta t = \Delta t_{\max}/5$ and $\Delta t_{\max} = 0.368\,112\Delta l/c$ have been used and all the dispersion curves are subtracted by the linear dispersion relation for one-dimensional (1-D) simulations. Fig. 22 shows that the S-MRTD scheme with stencil 10 has a comparable performance to the 16th-order Yee's scheme. The addition of zero-resolution wavelets for the same stencil significantly improves the dispersion characteristics of the MRTD scheme. In this case, the dynamic range of ω is extended by approximately 90% and compares favorably even to the 22th-order Yee's scheme. This is expected due to the multiresolution-analysis principle that, for an arbitrary resolution n, the space W_n created by the wavelets is a subset of the space, which is orthogonal to that (S_n) created by the scaling functions of the same resolution; thus, the new basis composed by both scaling and wavelet functions spans a larger ("more complete") subspace of R than the scaling functions alone. Both S-MRTD and Wo-MRTD schemes have identical numerical phase errors up to the point that the S-MRTD scheme starts diverging (Fig. 23). As the stencil size of the Wo-MRTD scheme is increasing from 6 to 12 (see Fig. 24 and 25), the oscillatory variation of the phase error

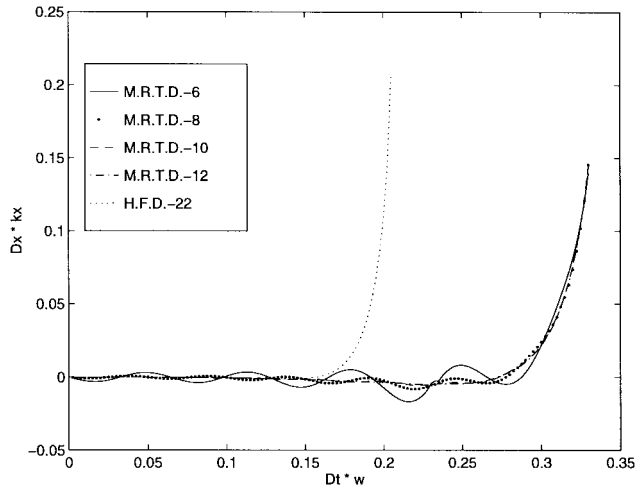

Fig. 24. Comparison of the oscillations of Wo-MRTD scheme for different stencil size.

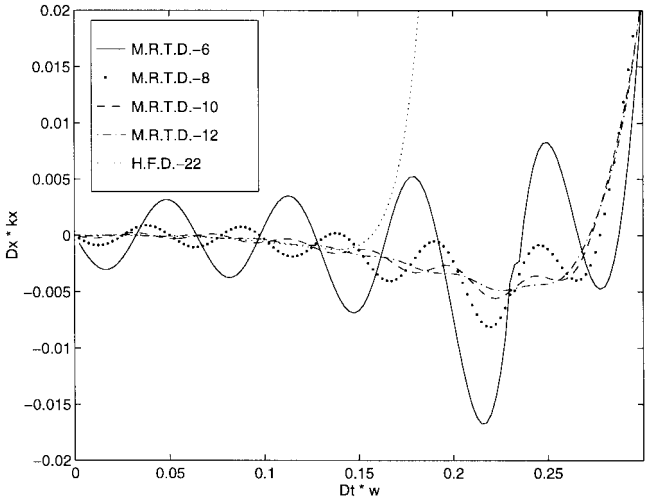

Fig. 25. Details of Fig. 22.

is diminishing to a negligible level generating an almost flat algorithm similar to the higher order Yee's ones.

As a conclusion, due to the poor dispersion performance of the FDTD technique even for ten cells/wavelength a normal-to-coarse grid is always required to avoid significant pulse distortions, especially for the higher spatial-frequency components. MRTD offers low dispersion even for sparse grids very close to the Nyquist limit.

IV. Conclusion

The stability and dispersion performance of the recently developed Battle–Lemarie MRTD schemes has been investigated for different stencil sizes and for zero-resolution wavelets. Analytical expressions for the maximum stable time step have been derived. Larger stencils decrease the numerical phase error making it significantly lower than FDTD for low and medium discretizations. Stencil sizes greater than ten offer a smaller phase error than FDTD even for discretizations close to 50 cells/wavelength. The enhancement of wavelets further improves the dispersion performance for discretizations close to the Nyquist limit (2–3 cells/wavelength) making it comparable to that of much denser grids, though it decreases the value of the maximum time step guaranteeing the stability of the scheme.

Acknowledgment

The authors would also like to thank C. Sarris for his remarks for the manuscript.

References

[1] K. S. Yee, "Numerical solution of initial boundary value problems involving Maxwell's equations in isotropic media," *IEEE Trans. Antennas Propagat.*, vol AP-14, pp. 302–307, May 1966.
[2] A. Taflove and M. E. Brodwin, "Numerical solution of steady-state electromagnetic scattering problems using the time-dependent Maxwell's equations," *IEEE Trans. Microwave Theory Tech.*, vol. MTT-23, pp. 623–630, Sept. 1975.
[3] M. Krumpholz and L. P. B. Katehi, "MRTD: New time-domain schemes based on multiresolution analysis," *IEEE Trans. Microwave Theory Tech.*, vol. 44, pp. 555–561, Apr. 1996.
[4] A. Taflove, *Computational Electrodynamics*. Norwood, MA: Artech House, 1995.
[5] K. L. Shlager and J. B. Schneider, "Analysis of the dispersion properties of the multiresolution time-domain method," in *Proc. IEEE AP-S*, vol. 4, 1997, pp. 2144–2147.
[6] W. Y. Tam, "Comments on "New prospects for time domain analysis," *IEEE Microwave Guided Wave Lett.*, vol. 6, pp. 422–423, Nov. 1996.

Emmanouil M. Tentzeris (S'89–M'82) was born in Piraeus, Greece, in 1970. He received the electrical engineering and computer science diploma degree (*suma cum laude*) from the National Technical University of Athens (NTUA), Athens, Greece, in 1992, and the M.Sc. and Ph.D. degrees from The University of Michigan at Ann Arbor, Ann Arbor, in 1993 and 1998, respectively.

From 1992 to 1998, he was a Graduate Research Assistant in the Radiation Laboratory, The University of Michigan at Ann Arbor. He is currently an Assistant Professor with the Electrical and Computer Engineering Department, Georgia Institute of Technology, Atlanta. He has authored or co-authored over 35 papers in refereed journals and conference proceedings. His research interests include the development of novel numerical techniques and the application of the principles of multiresolution analysis in the simulation of microwave circuits used in wireless or satellite communication systems.

Dr. Tentzeris is a member of The Technical Chamber of Greece. He was awarded the 1997 Best Paper Award presented by the International Microelectronics and Packaging Society.

Robert L. Robertson was born in Fairfax, VA, in 1971. He received the B.S.E.E. degree from the University of Wisconsin, Madison, in 1995, the M.S.E.E. degree from the University of Michigan at Ann Arbor, in 1997, and is currently working toward the Ph.D. degree at The University of Michigan at Ann Arbor.

He is currently a Graduate Research Assistant with the Radiation Laboratory, The University of Michigan at Ann Arbor. His research interests include the development of time-domain analysis techniques used in the analysis of antennas and wireless communication systems.

Mr. Robertson is a member of Eta Kappa Nu.

James F. Harvey (M'91) is currently a Research Program Manager at the Army Research Office, Research Triangle Park, NC, with primary responsibility for the fields of EM's, antennas and antenna structures, innovative microwave and millimeter-wave circuit integration, low-power/minimum-power system design, and landmine detection. His programs include a focus on small multifrequency multifunctional antennas for U.S. Army vehicles, radio propagation over complex terrain affecting data communications, and new millimeter-wave circuit integration techniques such as spatial power combining, micromachining, and advanced EM calculational techniques. His personal research interests are in the fields of quasi-optics and multiresolution analysis of EM structures.

Linda P. B. Katehi (S'81–SM'85–F'95) received the B.S.E.E. degree from the National Technical University of Athens, Athens, Greece, in 1977, and the M.S.E.E. and Ph.D. degrees from the University of California at Los Angeles, in 1981 and 1984, respectively.

In September 1984, she joined the faculty of the Electrical Engineering and Computer Science Department, The University of Michigan at Ann Arbor, where she is currently an Associate Dean of Graduate Education and Professor of electrical engineering and computer science. She has been interested in the development and characterization (theoretical and experimental) of microwave, millimeter printed circuits, the computer-aided design of very large scale integration (VLSI) interconnects, the development and characterization of micromachined circuits for millimeter-wave and submillimeter-wave applications, and the development of low-loss lines for terahertz-frequency applications. She has also been theoretically and experimentally studying various types of uniplanar radiating structures for hybrid-monolithic oscillator and mixer designs.

Dr. Katehi is a member of IEEE AP-S and MTT-S, Sigma XI, Hybrid Microelectronics, and URSI Commission D. From 1992 to 1995, she was a member of the IEEE AP-S AdCom. She is an associate editor for the IEEE TRANSACTIONS OF THE MICORWAVE THEORY AND TECHNIQUES. She was awarded the 1984 IEEE AP-S W. P. King Best Paper Award, the 1985 IEEE AP-S A. Schelkunoff Best Paper Award, the NSF Presidential Young Investigator Award, a 1987 URSI Young Scientist Fellowship, the Humboldt Research Award, 1994 University of Michigan Faculty Recognition Award, and the 1996 IEEE MTT-S Microwave Prize.